New Observations of Solar Wind $1/f$ Turbulence Spectrum from Parker Solar Probe

Zesen Huang (黄泽森) [1], Nikos Sioulas [1], Chen Shi (时辰) [1], Marco Velli,[1,2] Trevor Bowen [3],
Nooshin Davis [4], B. D. G. Chandran [4], Ning Kang (康宁) [5], Xiaofei Shi (石晓霏) [1], Jia Huang (黄佳) [3],
Stuart D. Bale [6,3], J. C. Kasper [7,8], Davin E. Larson [9], Roberto Livi [9], P. L. Whittlesey [9],
Ali Rahmati [9], Kristoff Paulson [10], M. Stevens [10], A. W. Case [10], Thierry Dudok de Wit [11],
David M. Malaspina [12,13], J.W. Bonnell [3], Keith Goetz [14], Peter R. Harvey [3], and
Robert J. MacDowall [15]

[1]*Department of Earth, Planetary, and Space Sciences, University of California, Los Angeles, CA, USA*
[2]*International Space Science Institute, Bern 3012, CH*
[3]*Space Sciences Laboratory, University of California, Berkeley, CA 94720-7450, USA*
[4]*Space Science Center and Department of Physics, University of New Hampshire, Durham, NH 03824, USA*
[5]*Department of Atmospheric and Oceanic Sciences, University of California, Los Angeles, CA, USA*
[6]*Physics Department, University of California, Berkeley, CA 94720-7300, USA*
[7]*BWX Technologies, Inc., Washington DC 20001, USA.*
[8]*Climate and Space Sciences and Engineering, University of Michigan, Ann Arbor, MI 48109, USA.*
[9]*Space Sciences Laboratory, University of California, Berkeley, CA 94720, USA.*
[10]*Smithsonian Astrophysical Observatory, Cambridge, MA 02138 USA.*
[11]*LPC2E, CNRS and University of Orléans, Orléans, France*
[12]*Astrophysical and Planetary Sciences Department, University of Colorado,*
Boulder, CO, USA
[13]*Laboratory for Atmospheric and Space Physics, University of Colorado,*
Boulder, CO, USA
[14]*School of Physics and Astronomy, University of Minnesota, Minneapolis, MN 55455, USA*
[15]*Solar System Exploration Division, NASA/Goddard Space Flight Center, Greenbelt, MD, 20771*

ABSTRACT

The trace magnetic power spectrum in the solar wind is known to be characterized by a double power law at scales much larger than the proton gyro-radius, with flatter spectral exponents close to -1 found at the lower frequencies below an inertial range with indices closer to $[-1.5, -1.6]$. The origin of the $1/f$ range is still under debate. In this study, we selected 109 magnetically incompressible solar wind intervals ($\delta|\boldsymbol{B}|/|\boldsymbol{B}| \ll 1$) from Parker Solar Probe encounters 1 to 13 which display such double power laws, with the aim of understanding the statistics and radial evolution of the low frequency power spectral exponents from Alfvén point up to 0.3 AU. New observations from closer to the sun show that in the low frequency range solar wind turbulence can display spectra much shallower than $1/f$, evolving asymptotically to $1/f$ as advection time increases, indicating a dynamic origin for the $1/f$ range formation. We discuss the implications of this result on the Matteini et al. (2018) conjecture for the $1/f$ origin as well as example spectra displaying a triple power law consistent with the model proposed by Chandran et al. (2018), supporting the dynamic role of parametric decay in the young solar wind. Our results provide new constraints on the origin of the $1/f$ spectrum and further show the possibility of the coexistence of multiple formation mechanisms.

Keywords: Magnetohydrodynamics(MHD); Solar Wind; Plasmas; Turbulence; Waves

1. INTRODUCTION

The trace magnetic power spectrum (PSD) in the solar wind is often characterized by a double power law from intermediate to large scales, with power spectral exponents in the inertial range around -5/3 (or closer to

-3/2 in the inner heliosphere) and -1 at larger scales, respectively. This double power law is usually found in the fast wind (Bavassano et al. 1982; Denskat & Neubauer 1982; Burlaga & Goldstein 1984), and has only been recently observed in very long intervals of slow wind

(Bruno et al. 2019). The low frequency (large scale) range of the spectrum has been considered as the energy reservoir that facilitates the turbulence cascade in the solar wind. The origin and formation mechanism of the $1/f$ range of the PSD is still not well-understood and under active debate (see e.g. Matthaeus & Goldstein (1986); Velli et al. (1989); Dmitruk & Matthaeus (2007); Verdini et al. (2012); Matteini et al. (2018); Chandran (2018); Magyar & Doorsselaere (2022)). It is worth noting that the $1/f$ range of the spectrum is indicative of a scale-independent fluctuation energy distribution, i.e. equipartition of energy over all scales (Keshner 1982).

The majority of the models proposed for the double power law were built on an *a priori* assumption of the existence of $1/f$ spectrum at large scales with few notable exceptions. For example it has been pointed out by Chandran (2018) (henceforth denoted as C18) that in Fig 2-2 of Tu & Marsch (1995), the low frequency z^+ (Elsasser variables: $z^\pm = V \mp B/\sqrt{\mu_0 \rho}$) spectrum were as shallow as $f^{-0.5}$ in the low frequency range, which C18 referred as 'infrared' range. C18 used this as an input to the model and the parametric decay induced inverse cascade of outward propagating Alfvén wave would eventually produce a triple power law z^+ spectrum with $1/f$ in the middle frequency range between 'infrared' range and the inertial range.

Another example would be the conjecture proposed by Matteini et al. (2018) (henceforth denoted as M18) which tried to build a connection between spectral properties and magnetic compressibility. In particular, there's a paradox between an arbitrary power law index and low magnetic compressibility at all scales. Their conjecture shows that, for turbulence with low magnetic compressibility, if the magnetic fluctuations fully saturate over the scales, i.e. $\langle \delta B \rangle = \langle \delta \boldsymbol{B} \rangle \sim |B| = B$, we have $\langle \delta B/B \rangle \sim \langle \delta B \rangle / B \sim 1$. According to the well-known relation which connects the slope in the power spectrum $P(k) \propto k^\alpha$, and the exponent in the second order structure function $\delta B^2 \propto l^{-2\beta}$ via: $\alpha = 2\beta - 1$, $-3 < \alpha < -1$ (see e.g. (Monin & Jaglom 1987)), we see that when $\langle \delta B/B \rangle \sim 1$ for sufficiently large scales (Note that $\langle \delta B/B \rangle$ is a function of scales l or temporal increment τ), we have $\beta \sim 0$, and hence $\alpha \gtrsim -1$, for the same scale range. Consequently, $1/f$ is the steepest possible realization of power spectrum when magnetic fluctuations fully saturate to the $\langle \delta B/B \rangle \sim 1$ state. In addition, their result leads to a straightforward connection between the scale l_0 at which magnetic field fluctuations fully saturate (i.e. $\langle \delta B/B \rangle \sim 1$) and the spectral breakpoint f_B of the double power law in PSD. M18 argued that closer to the sun, unless the $1/f$ range is formed in the solar corona and advected outwards pre-

serving its shape, it should gradually disappear moving closer to the sun where $\delta B/B < 1$.

Previous observations with *Ulysses*, *Helios*, *WIND* have only explored the heliosphere beyond 0.3 AU. It is well known that due to solar wind expansion, B decreases like R^{-2} radially per conservation of magnetic flux (or Parker Spiral (Parker 1958), because the field is mostly radial close to the sun) and δB decreases like $R^{-1.5}$ per WKB theory (see e.g. Whang (1973); Heinemann & Olbert (1980); Velli et al. (1991); Tu & Marsch (1995); Huang et al. (2022)), where R is heliocentric distance. And hence $\langle \delta B/B \rangle$ is expected to increase radially as $R^{0.5}$ from Alfvén critical point (where $\delta B^2, \delta V^2 \propto V_{sw}V_A/(V_A + V_{sw})^2$ reaches its absolute maximum per WKB theory. However, the peak is expected to locate inside the Alfvén point due to non-WKB effects, see e.g. Cranmer & Ballegooijen (2005); Verdini & Velli (2007); Chen et al. (2020); Bandyopadhyay et al. (2022)) until it reaches its full saturation at 1 around 0.3 AU. Therefore, closer to the sun, based on the WKB prediction, we expect to see magnetically incompressible intervals with partial saturation ($\langle \delta B/B \rangle \sim const, const < 1$), or without saturation ($\langle \delta B/B \rangle$ keeps increasing over scales but smaller than 1). It is hence important to validate the connection between $1/f$ spectrum and low magnetic compressibility with solar wind closer to the sun where full magnetic fluctuations saturation is not achieved.

As a consequence, with new observations much closer to the sun from Parker Solar Probe (PSP) (Fox et al. 2016), there are two major questions to be investigated: 1. What are the statistics and radial evolution of low frequency power spectral exponents; 2. With the new evidence from closer to the sun, what new constraints can be applied to the existing models of $1/f$ spectrum. To answer these questions we perform a systematic search for magnetically incompressible ($\delta|\boldsymbol{B}|/|\boldsymbol{B}| \ll 1$) solar wind intervals that are characterized by a double power law with PSP data from Encounter 1 to Encounter 13. The rest of the paper is organized as follows: In section 2, we explain the data selection and analysis procedure; In section 3, we show the main results; In section 4, we discuss the implications from new observations on Matteini et al. (2018) and Chandran (2018); In section 5, we conclude and summarize the main results.

2. DATA AND ANALYSIS PROCEDURES

In order to study the low frequency spectral properties of magnetically incompressible solar wind observed by PSP, we performed a systematic search for magnetically incompressible turbulence intervals from E1 (Nov 2018) to E12 (Jun 2022). We mainly use high-resolution vector magnetic field measurements from FIELDS in-
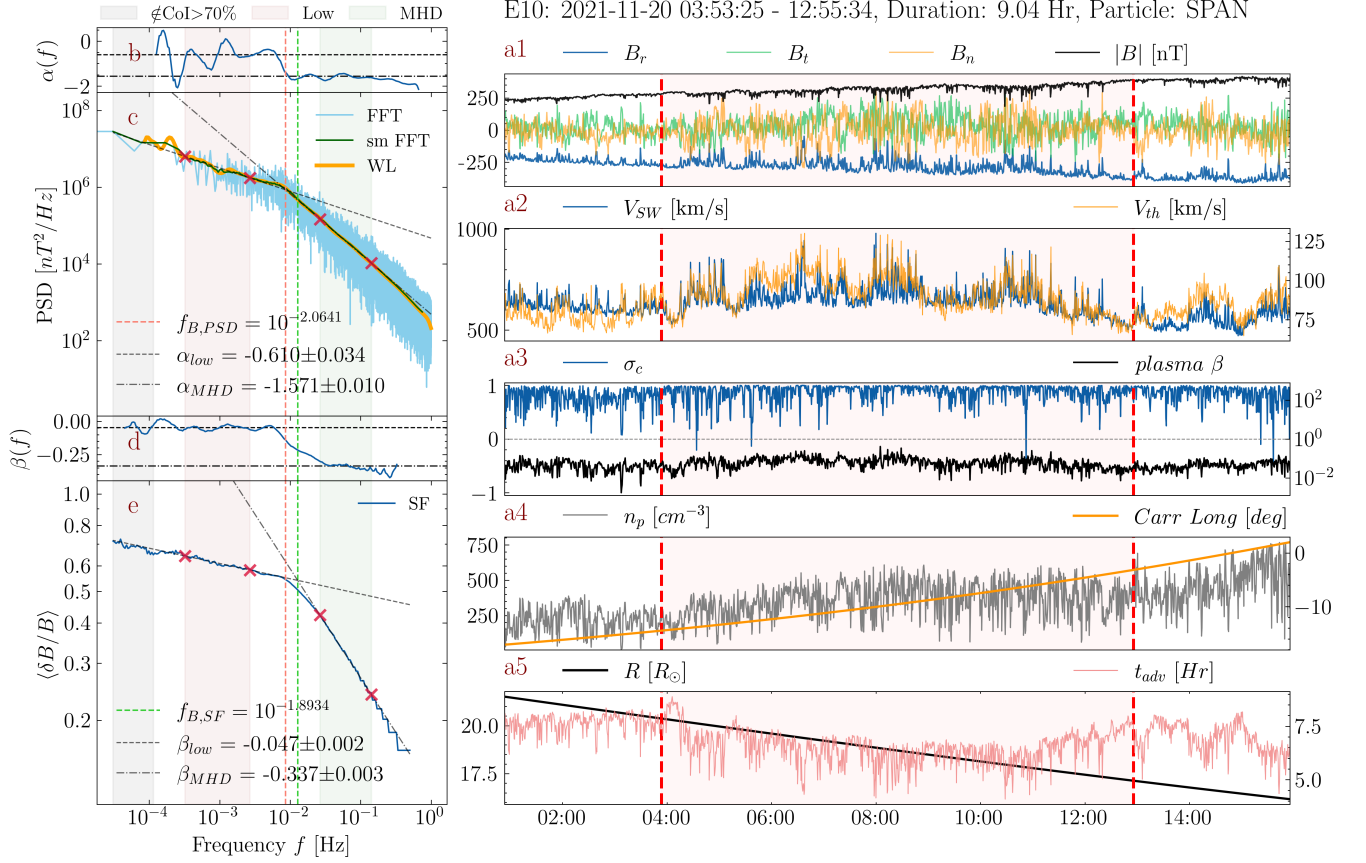
Figure 1. Example of a magnetically incompressible solar wind interval from PSP Encounter 10, close to the perihelion. The particle data of this interval are provided by SPAN (Livi et al. 2022). (a1-a5) show time series of magnetic field B_{rtn} in RTN coordinates; solar wind speed V_{SW} and solar wind thermal speed V_{th}; cross helicity σ_c and plasma beta β; proton density n_p and Carrington longitude; and heliocentric distance R in solar radii $R_{\odot}$ and advection time $t_{adv} = R/V_{SW}$, respectively. The selected interval is indicated with the red shaded area enclosed by two red dashed lines. (b) Power law fitting index α as a function of frequency f of trace PSD. (c) Fast Fourier Transformation (FFT) is plotted in blue as background, smoothed FFT PSD is the green line, and Morlet Wavelet Transformation (WL) PSD is the orange line. The two pairs of red crosses accompanied with red and green shaded areas indicate the ranges of frequency over which the power-law fits are applied, and the two fitted lines are shown in dashed and dashed-dot lines. The gray shaded area is the frequency range where more than 70% of points fall out of the Cone of Influence (CoI) of wavelet transformation. The red dashed line indicates the intersect of two fitted lines, interpreted as the low frequency break point. (d) Power law fitting index β as a function of frequency f of the normalized structure function SF. (e) Normalized first order structure function $\langle \delta B/B \rangle$ as a function of frequency $f = 1/(2*\Delta t)$, where Δt is the temporal increment. Two fits are applied to the same frequency ranges from (c), which produce a similar low frequency break point, indicated by the green dashed line.

struments (Bale et al. 2016) to calculate the magnetic turbulence spectrum, and proton measurements from SWEAP instruments (Kasper et al. 2016) and Quasi Thermal Noise (QTN) electron density measurements (Moncuquet et al. 2020; Pulupa et al. 2017) to support interval selection.

2.1. *Interval Selection*

Our selection of magnetically incompressible solar wind intervals is based on the evaluation of the scale-dependent magnetic compressibility $\eta_B(T)$:

$$\eta_B(T) = \left\langle \frac{|B| - \langle |B| \rangle_T}{\langle B \rangle} \right\rangle \qquad (1)$$

where $\langle \rangle_T$ is the ensemble average at scale T. For all intervals, we ensure that η_B is smaller than 0.1 for any given scale T. Moreover, due to the rapid movement of the spacecraft around perihelia, careful selection is needed to ensure that the spacecraft stays within the same type of solar wind over the selected interval. Therefore secondary parameters, including solar wind speed $V_{sw} = |V|$, thermal speed $V_{th} = \sqrt{2k_BT/m_p}$, normalized cross helicity $\sigma_c = (z^{+2} - z^{-2})/(z^{+2} + z^{-2})$, plasma $\beta = 2\mu_0 P/B^2$, proton density n_p, Carrington longitude, Heliocentric distance R, and advection time $t_{adv} = R/V_{sw}$ are examined to differentiate different solar types (see Figure 1 panels a1-a5). With our selection

4

criteria, we ended up with 109 non-overlapping magnetically incompressible solar wind intervals observed by PSP from E1 to E13, with total 1500 hours worth of data (see Figure 2c for histogram of interval lengths). Note that the jets in the solar wind speed in panel a2, which are accompanied with partial or total reversal of B_r in panel a1 are known as switchbacks, and have been studied by numerous recent studies (see e.g. Bale et al. (2019); Dudok de Wit et al. (2020); Tenerani et al. (2020); Farrell et al. (2020); Mozer et al. (2020); Woolley et al. (2020); Bourouaine et al. (2020); Martinović et al. (2021); Larosa et al. (2021); Tenerani et al. (2021); Hernández et al. (2021); Laker et al. (2021); Meng et al. (2022); Shi et al. (2022b); Huang et al. (2023) and references therein). They are known as large amplitude or spherically polarized Alfvén wave (Mallet et al. 2021; Mallet & Chandran 2021) with almost constant magnetic modulus.

2.2. *Diagnostics: Magnetic Trace Power Spectrum and Structure Function*

For each interval, the following two diagnostics are calculated: trace power spectrum density (PSD) and normalized first-order structure function (SF) for vector magnetic field. To produce a reliable low frequency turbulence spectrum, for each interval, we calculate the trace power spectrum density (PSD) with both Morlet Wavelet Transformation (WL) and Fast Fourier Transformation (FFT). For FFT, we smooth the spectrum by averaging over a sliding window of a factor of 2 in the frequency domain (sm-FFT). The smooth spectra calculated with the two methods (WL and sm-FFT) generally overlap with each other perfectly in the high frequency range but gradually deviate from each other at the low frequency end. Therefore, we keep the spectrum up to the frequency where more than 70% of points fall out of the Cone of Influence (CoI) of the WL spectrum, and we trust only the frequency range where WL overlap with sm-FFT. We calculate the power law fit index α by fitting on the WL PSD unless specified otherwise, and henceforth referred simply as PSD.

We follow the steps described in M18 to calculate the normalized first-order structure function for vector magnetic field. We apply 200 logarithmically spaced lags Δt as temporal increment of vector magnetic field $\delta \boldsymbol{B}(t, \Delta t) = \boldsymbol{B}(t) - \boldsymbol{B}(t + \Delta t)$ within the range $(1s, length\ of\ interval/2)$. The normalized first-order structure function is then calculated by:

$$SF(\Delta t) = SF_{norm}(\Delta t) = \left\langle \frac{|\delta \boldsymbol{B}(t, \Delta t)|}{B(t, \Delta t)} \right\rangle_t \quad (2)$$

where we denote $|\delta \boldsymbol{B}|$ as δB and $|\boldsymbol{B}|$ as B, and $\langle \rangle_t$ is average with regard to t for scale Δt. Note that the

intervals we select are magnetically incompressible, and hence B can be considered as scale-independent and can be taken out of the averaging window $\langle \rangle_t$. The resultant $SF(\Delta t)$ in the temporal domain is finally converted to $SF(f)$ in the frequency domain via $f = 1/(2 \cdot \Delta t)$ because a half period in the absolute fluctuation corresponds to the full period in the non-absolute one.

To extract spectral information from PSD, we apply power law fit on PSD in both low and MHD inertial frequency ranges where the spectrum stabilize visually (red and green shaded area in Figure 1c), and we obtain two power law fits with indices α_{Low} and α_{MHD} (black dashed line and dashed dotted line in Figure 1c). The intersect of the two fit lines is interpreted as the low frequency break point ($f_{B,PSD}$, red dashed line). To compare the spectral properties of PSD and SF, we apply power law fit in the same frequency ranges to SF (extended shaded area in Figure 1e), and the intersect of two fit lines is also interpreted as the low frequency break point ($f_{B,SF}$, green dashed line). Clearly the two break frequencies $f_{B,PSD}$ and $f_{B,SF}$ are very close to each other, consistent with M18. The small deviation may be attributed to spectral leakage of the structure function, which leads to a spectrum smoother than the wavelet or PSD result. For completeness, two moving fits $\alpha(f)$ and $\beta(f)$ with window size of 1/3 decade on PSD and SF are shown in Figure 1b and 1d.

3. RESULTS

3.1. *Statistics of Power Spectral Exponents*

For the 109 intervals, power law fit is applied to both high frequency (MHD/inertial) and low frequency ranges with the method described in section 2.2. The primary statistical results are presented in Figure 2a, in a style similar to Figure 6 in Bruno et al. (2019). The histogram of power law fit index in the MHD inertial range α_{MHD} is shown in dark red. Most of the intervals have an inertial range spectral exponent that falls within the expected value range [-1.67, -1.5], predicted by many existing phenomenologies (Kolmogorov 1941; Iroshnikov 1964; Kraichnan 1965; Sridhar & Goldreich 1994; Goldreich & Sridhar 1997; Boldyrev 2005, 2006), consistent with recent observations (see e.g. Chen et al. (2020); Telloni et al. (2021); Shi et al. (2021); Kasper et al. (2021); Zank et al. (2022); Sioulas et al. (2023a,b); Raouafi et al. (2023)). However, for the low frequency range fit index (α_{Low}, dark blue), the spectral exponents have an unexpectedly wide distribution, and the majority of them are larger than -1, i.e. the corresponding low frequency spectra are shallower than $1/f$.
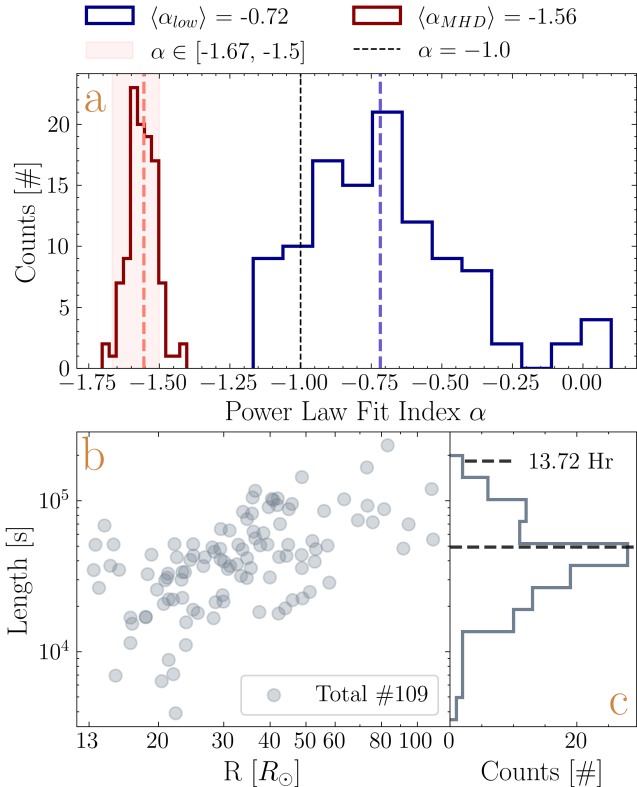
Figure 2. (a) Histograms of power law fit index α of low frequency (blue) and MHD frequency (red) ranges. The averaged index values are indicated with corresponding dashed lines and are shown in the legends. The expected power spectral exponent value range from various phenomenologies is indicated with red shaded area. (b) Statistics of length and mean radial distance of the selected 109 intervals. (c) Histogram of interval lengths. The average length is 13.72 hours, with minimum of 1.08 hours and maximum of 64.70 hours.

3.2. *Radial Evolution and Dependence on Solar Wind Speed*

The radial evolution of power law fit index of PSD in the low frequency range α_{Low} is shown in Figure 3, sorted with advection time $t_{adv} = R/V_{SW}$ in 3a and heliocentric distance R in 3b. To display the trend of evolution, a binned average weighted with interval length is plotted on top of the scatters. When we sort the intervals with advection time t_{adv}, a clear asymptotic evolution from shallower spectrum towards $1/f$ spectrum is seen. However, when sorted with heliocentric distance R, no clear trend is found, and instead α_{Low} is scattered in a wide range of values below 0.3 AU. For completeness, the dependence of α_{Low} on solar wind speed is shown in panel c. For intervals with very low solar wind speed (~ 200 km/s), which are typically observed very close to the sun, α_{Low} are mostly close to -1, i.e. very

close to $1/f$ spectrum. For intervals with higher solar wind speed, no obvious trend is observed. Therefore, for the very low speed streams, it is possible that the $1/f$ spectrum originated from the solar corona (see e.g. Matthaeus & Goldstein (1986)).

However, substantial solar wind acceleration has been observed below 0.3 AU (see e.g. Shi et al. (2021); Sioulas et al. (2022); Shi et al. (2022a)). In other words, the solar wind speed is a radially varying parameter even for the same stream, and hence the dependence of α_{Low} on solar wind speed should be taken with caution. Moreover, it should be also noted that the actual advection time is an integrated quantity, and thus the t_{adv} used here can be merely considered as a proxy to the real advection time.

4. DISCUSSIONS

4.1. *Implications on Matteini2018*

M18 tried to build a connection between low magnetic compressibility and $1/f$ spectrum via the well-known relation: $\alpha = 2\beta - 1$, $-1 > \alpha > -3$, where α is the spectral exponent of the PSD, and β is the power law index of the first order structure function (here expressed in terms of frequency). Due to low magnetic compressibility, $\langle \delta B/B \rangle$ can be considered as first order structure function δB normalized by its own constant modulus. Therefore the fully saturated magnetic fluctuations, i.e. $\delta B/B \sim 1$, can be translated to $\beta \sim 0$, and therefore $\alpha \gtrsim -1$. In other words, $1/f$ is the steepest possible realization of the low frequency spectrum when magnetic field fluctuations fully saturates. It has also been proposed by M18 that "unless the $1/f$ range is formed in the corona and just advected in interplanetary space preserving its shape, it should gradually disappear, moving closer to the Sun where $\delta B/B < 1$."

It is therefore interesting to examine the behaviors of α_{Low} and β_{Low} closer to the sun where $\delta B/B < 1$. There are roughly two possible behaviors of $\langle \delta B/B \rangle$ in the low frequency range: 1. Partial saturation, i.e. $\delta B/B \sim const$, $\beta \sim 0$; 2. No saturation, $\beta < 0$. Figure 4a shows the histogram of the β_{Low} and β_{MHD} in both low and MHD frequency ranges. The histogram of β_{Low} clearly shows that substantial portion of intervals have no saturation ($\beta \lesssim -0.1$). However, the scatter plot of $(\beta_{Low}, \alpha_{Low})$ in Figure 4b shows that the low frequency PSD of these intervals are close to $1/f$. In fact for those intervals with partial saturation ($\beta_{Low} \gtrsim -0.1$), the scatter plot shows that the corresponding α_{Low} are much greater than -1, i.e. the low frequency PSD are much shallower than $1/f$.

Figure 4b further reveals that in the inertial range, the observed (β, α) pairs follow the relation $\alpha = 2\beta - 1$
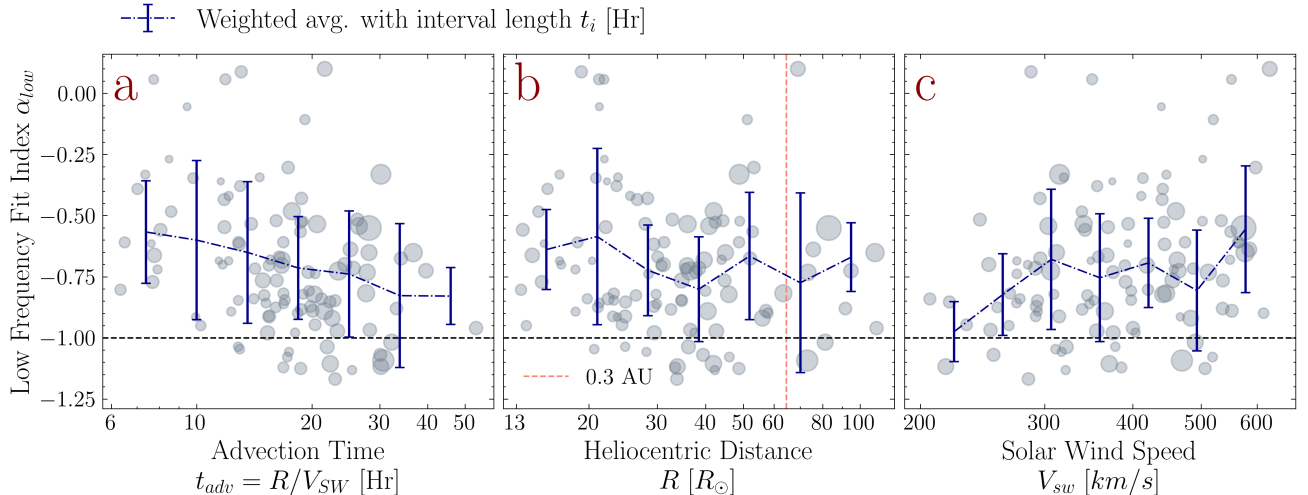
Figure 3. (a) Radial evolution of low frequency power law fit index α_{Low}, sorted with advection time ($t_{adv} = R/V_{SW}$). The sizes of the circles indicate the interval length (weight), and the line plot is the binned weighted average of α_{Low}. The errorbars are one standard error of α_{Low} from each bin. (b) Radial evolution of α_{Low} sorted with Heliocentric distance R. (c) Dependence of α_{Low} on solar wind speed V_{SW}.

pretty well (black dashed line), with a slight systematic shift towards shallower α, but in the low frequency range deviate significantly. To understand such deviation, we generate 1-D artificial time series with different power spectral exponent α_0. For each α_0, we generate an artificial time series $A(t; \alpha_0)$ formed with sinusoidal fluctuations with random phases and amplitudes following power law:

$$A(t; \alpha_0) = \sum_i^N \omega_i^{(\alpha_0+1)/2} \sin[2\pi(\omega_i t + \phi_i)] \qquad (3)$$

where ω_i is i^{th} frequency log-linearly spaced from 10^{-5} Hz to 1 Hz, ϕ_i is random phase in range of $(0, 2\pi)$, and N is set to 10000. For each $A(t; \alpha_0)$, we calculate the power law fitting index for the PSD (α) and SF (β) from the same frequency range $(10^{-2.5}, 10^{-1})$ Hz.

The scatter plot of $(\alpha, \beta)_{Artificial}$ pairs are shown in Figure 4b as gray crosses. $(\alpha, \beta)_{Artificial}$ catch well the trend of the observed (α, β) pairs, especially in the MHD frequency range, and also deviate significantly from the relation $\alpha = 2\beta - 1$. Such systematic deviation is possibly due to the spectral leakage effect, because contrary to FFT and wavelet transformation, the structure function has a broad-band response. Therefore, cautions should be taken when one is trying to relate $1/f$ spectrum with magnetic fluctuations saturation (regardless of full or partial). For completeness, shown in Figure 4c, for those 55 intervals with partially saturated magnetic fluctuations (here defined as $\beta > -0.07$), we see the radial evolution of saturation values $\langle \delta B/B \rangle$ follows well with the WKB prediction of $R^{0.5}$.

In summary, one should be careful when relating magnetic fluctuations saturation ($\langle \delta B/B \rangle \sim const$) to $1/f$ spectrum, because of the spectral leakage effect. And closer to the sun where $\delta B/B < 1$, we see low frequency spectra much shallower than $1/f$ with partially saturated magnetic fluctuations. One good example has already been shown in Figure 1. Therefore, according to M18, it is possible that some of these low frequency range spectra originated from the solar corona.

4.2. Implications on Chandran2018

C18 proposed that the $1/f$ spectrum is formed by inverse cascade of Alfvén waves facilitated by parametric decay within the context of weak-turbulence theory. The author initialize the simulation with primarily outward propagating Alfvén waves, i.e. $e^+ \gg e^-$, where $e^\pm$ are the frequency (f) spectra of Alfvén waves propagating in opposite directions along the magnetic field lines. If the initial e^+ has a peak frequency f_0 (where fe^+ is maximized), and an 'infrared' scaling f_p at smaller f with $-1 < p < 1$, then e^+ acquires an f^{-1} scaling throughout a range of frequencies that spreads out in both directions from f_0. The final state of their model evolution is a triple power law with 'infrared' scaling in the low frequency, $1/f$ in the intermediate frequency range, and f^{-2} scaling in the inertial range (the inertial range is initialized with the critical-balanced parallel spectrum of $k_\parallel^{-2}$, see e.g. Goldreich & Sridhar (1995); Podesta (2009); Forman et al. (2011)).

Therefore it is interesting to explore the magnetically incompressible (yet weakly compressible to allow parametric decay), Alfvénic turbulence (primarily outward propagating Alfvén waves, i.e. $|\sigma_c| \sim 1$) intervals close
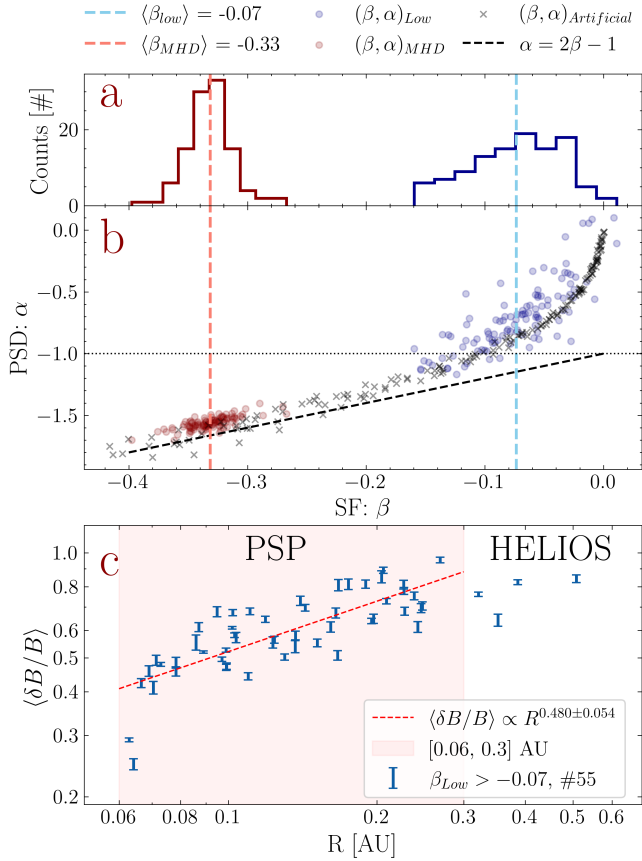
Figure 4. (a) Histogram of power law fit index β of the normalized first order structure function SF from both low (blue) and MHD (red) frequency ranges. The averages are indicated with corresponding dashed lines. (b) Scatters of power law fit index pairs (α,β) of trace PSD and SF from both low (blue) and MHD (red) frequency ranges. The (α,β) pairs from artificial data are also shown with black crosses, and the theoretical relation $\alpha = 2\beta-1$ is indicated with black dashed line. (c) Dependence of $\langle\delta B/B\rangle$ from the saturated intervals $(\beta_{Low} > -0.07)$ on Heliocentric distance R. The value ranges of $\langle\delta B/B\rangle$ in the low frequency range are indicated with errorbars. The newly explored Heliosphere radial range $(R < 0.3\ AU)$ is indicated with red shaded area.

to the sun, to see if there exists the triple power law z^+ spectrum. Among the 109 intervals, there are 4 intervals displaying clear triple power law in trace z^+ PSD with stable intermediate frequency range. One of the best examples is shown in Figure 5, which is an interval from E12, with $\langle\sigma_c\rangle = 0.82$. Note that due to the low resolution particle data, the time series is resampled to 5s, and hence the WL spectrum is very wavy. To acquire a better moving fit $\alpha(f)$ profile, the moving power law fit with window size of 1/3 decade is applied to the smoothed FFT PSD (green line).

In the low frequency range, we see a stable 'infrared' spectrum with $f^{-0.627}$. In the intermediate range, the
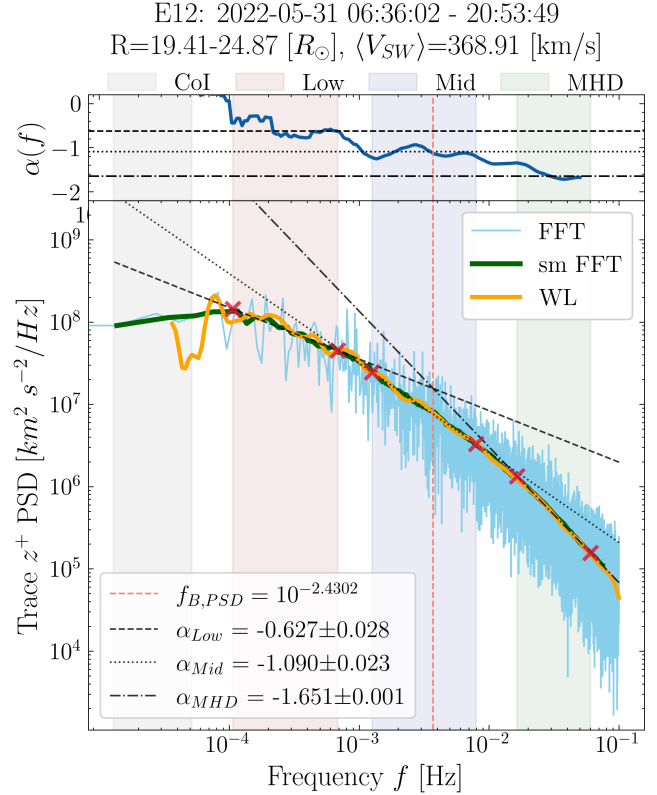
Figure 5. Example of C18 type of trace z^+ spectrum. The FFT spectrum is shown with blue line as background, the smoothed FFT is the green line, and the trace Morlet Wavelet (WL) PSD is the orange line. The gray shaded area indicates that more than 70% of points fall out of the Cone of Influence (CoI) of wavelet transformation. The power law fit is conducted on the smoothed FFT, and the moving window fit $\alpha(f)$ (window sized 1/3 decade) is shown in the overhead panel. The trace PSD is separated into three distinct frequency ranges (Low, Mid, MHD), each possesses a quasi-steady power law range, indicated with red (Low), blue (Mid), and green (MHD) shaded areas. Power law fits are applied to each of the ranges and the fit indices $\alpha_{Low/Mid/MHD}$ are shown in the legends. A "low frequency break" is found as the intersect between the power law fits from low frequency and MHD inertial range, indicated with orange dashed line.

spectrum is very close to $1/f$. And in the inertial range, the scaling is agreeable with the perpendicular spectrum of $f^{-5/3}$ predicted by the critical balance theory, which would mask the steeper parallel spectrum because we are observing the trace z^+ PSD. This is supported Sioulas et al. (2023b), which has shown that when considering turbulence anisotropy, for fast streams $(V_{sw} \gtrsim 400km/s)$ close to the sun, the low frequency spectrum is dominated by parallel fluctuations, and in the inertial range, the perpendicular spectrum has a $f^{-5/3}$ scaling. This is also consistent with the simulation

by Verdini et al. (2012), where at higher frequencies the steep parallel spectral slope (-2) is masked by the more energetic perpendicular spectrum (slope -5/3). In summary, this triple power law is consistent with the simulation result from C18, and further provide evidence for the presence of parametric decay instability in the solar wind (see e.g. Matteini et al. (2010); Tenerani & Velli (2013); Zanna et al. (2015); Tenerani et al. (2017); Shi et al. (2017); Bowen et al. (2018); Réville et al. (2018)).

It should also also noted that due to the existence of the triple power law, the concept of 'low frequency break point' is now questionable. For example the orange dashed line in Figure 5 is obtained as the intersect between the low frequency 'infrared' spectrum and the MHD spectrum, and interpreted as the low frequency break point $f_{B,PSD}$. However, any frequencies in between these two ranges should be considered as the 'break frequency'. Therefore, the low frequency break point obtained with this method would have a unacceptably large uncertainty. For this reason, we have not shown any statistics of $f_{B,PSD}$ in this study.

5. CONCLUSIONS AND SUMMARY

In this letter we have selected 109 magnetically incompressible intervals with total 1500 hours worth of data from Parker Solar Probe encounter 1 to 13. All of the intervals display double power law in the intermediate to large scales in their trace magnetic power spectrum density (PSD). Traditionally, the double power law in PSD is characterized by power indices $-5/3$ and -1 at the two scale ranges respectively, and there are many models in the literatures to explain the origin of the $1/f$ range (e.g. Matthaeus & Goldstein (1986); Velli et al. (1989); Dmitruk & Matthaeus (2007); Verdini et al. (2012); Matteini et al. (2018); Chandran (2018); Magyar & Doorsselaere (2022)). Previous observations from *Ulysses, Helios, WIND* have only explored the heliosphere beyond 0.3 AU. In this study, we aim to use the latest observations from PSP to provide constraints on the origin of the $1/f$ range.

From the statistics of the 109 intervals, we found that within 0.3 AU, the majority the intervals display spectra that are much shallower than $1/f$ in the low frequency range. And as advection time $t_{adv} = R/V_{SW}$ increases, the low frequency power law fit index α_{Low} asymptotically approach -1. This suggests a dynamical formation

of such range from the Alfvén point up to 0.3 AU. However when sorted with heliocentric distance, no obvious evolution of α_{Low} is observed. Moreover, for those extremely slow solar wind streams which were observed very close to sun, the low frequency spectra scaling are very close to $1/f$. Therefore we can not rule out the possibility that the $1/f$ originated from the corona and are advected out (Matthaeus & Goldstein 1986).

Unlike other models, Matteini et al. (2018) and Chandran (2018) allow the low frequency spectrum to be shallower than $1/f$. In fact, as has been pointed out by Chandran (2018), it has been reported by Tu & Marsch (1995) that in the low frequency range, z^+ have spectrum as shallow as $f^{-0.5}$. The new observations provide evidence inconsistent with the conjecture by Matteini et al. (2018) because closer to the sun where $\delta B/B < 1$ the low frequency spectrum does not gradually disappear, but instead they are omnipresent. On the other hand, some Alfvénic intervals display clear triple power law in the z^+ spectra with $1/f$ scaling in the intermediate frequency range, and therefore support the model from Chandran (2018).

The new observations from Parker Solar Probe encounter 1 to 13 provide abundant new evidence for the origin of the $1/f$ spectrum. Unfortunately, up to this point none of the existing models can fully explain the observed behaviors of the solar wind low frequency turbulence spectrum. In fact, it is even not appropriate to call this part of the spectrum '$1/f$' spectrum because of the omnipresent shallower spectra observed closer to the sun. However, based on this study, the new evidence indicate that for different intervals from different solar wind conditions, the low frequency spectrum might have different formation mechanisms. Therefore we need to accumulate more observations from future PSP orbits to obtain a clearer picture of the low frequency turbulence spectrum.

REFERENCES

Angelopoulos, V., Cruce, P., Drozdov, A., et al. 2019, Space Science Reviews, 215, 9, doi: 10.1007/s11214-018-0576-4

Bale, S. D., Goetz, K., Harvey, P. R., et al. 2016, ßr, 204, 49, doi: 10.1007/s11214-016-0244-5

Bale, S. D., Badman, S. T., Bonnell, J. W., et al. 2019, Nature, 1, doi: 10.1038/s41586-019-1818-7

Bandyopadhyay, R., Matthaeus, W. H., McComas, D. J., et al. 2022, The Astrophysical Journal Letters, 926, L1, doi: 10.3847/2041-8213/ac4a5c

Bavassano, B., Dobrowolny, M., Fanfoni, G., Mariani, F., & Ness, N. F. 1982, Solar Physics, 78, 373, doi: 10.1007/BF00151617

Boldyrev, S. 2005, The Astrophysical Journal, 626, L37, doi: 10.1086/431649

—. 2006, Physical Review Letters, 96, 115002, doi: 10.1103/PhysRevLett.96.115002

Bourouaine, S., Perez, J. C., Klein, K. G., et al. 2020, \apjl, 904, L30, doi: 10.3847/2041-8213/abbd4a

Bowen, T. A., Badman, S., Hellinger, P., & Bale, S. D. 2018, The Astrophysical Journal, 854, L33, doi: 10.3847/2041-8213/aaabbe

Bruno, R., Telloni, D., Sorriso-Valvo, L., et al. 2019, Astronomy & Astrophysics, 627, A96, doi: 10.1051/0004-6361/201935841

Burlaga, L. F., & Goldstein, M. L. 1984, Journal of Geophysical Research: Space Physics, 89, 6813, doi: 10.1029/JA089iA08p06813

Chandran, B. D. G. 2018, Journal of Plasma Physics, 84, doi: 10.1017/S0022377818000016

Chen, C. H. K., Bale, S. D., Bonnell, J. W., et al. 2020, The Astrophysical Journal Supplement Series, 246, 53, doi: 10.3847/1538-4365/ab60a3

Cranmer, S. R., & Ballegooijen, A. A. v. 2005, The Astrophysical Journal Supplement Series, 156, 265, doi: 10.1086/426507

Denskat, K. U., & Neubauer, F. M. 1982, Journal of Geophysical Research: Space Physics, 87, 2215, doi: 10.1029/JA087iA04p02215

Dmitruk, P., & Matthaeus, W. H. 2007, Physical Review E, 76, 036305, doi: 10.1103/PhysRevE.76.036305

Dudok de Wit, T., Krasnoselskikh, V. V., Bale, S. D., et al. 2020, The Astrophysical Journal Supplement Series, 246, 39, doi: 10.3847/1538-4365/ab5853

Farrell, W. M., MacDowall, R. J., Gruesbeck, J. R., Bale, S. D., & Kasper, J. C. 2020, The Astrophysical Journal Supplement Series, 249, 28, doi: 10.3847/1538-4365/ab9eba

Forman, M. A., Wicks, R. T., & Horbury, T. S. 2011, The Astrophysical Journal, 733, 76, doi: 10.1088/0004-637X/733/2/76

Fox, N. J., Velli, M. C., Bale, S. D., et al. 2016, Space Science Reviews, 204, 7, doi: 10.1007/s11214-015-0211-6

Goldreich, P., & Sridhar, S. 1995, The Astrophysical Journal, 438, 763, doi: 10.1086/175121

—. 1997, \apj, 485, 680, doi: 10.1086/304442

Harris, C. R., Millman, K. J., van der Walt, S. J., et al. 2020, Nature, 585, 357, doi: 10.1038/s41586-020-2649-2

Heinemann, M., & Olbert, S. 1980, Journal of Geophysical Research: Space Physics, 85, 1311, doi: 10.1029/JA085iA03p01311

Hernández, C. S., Sorriso-Valvo, L., Bandyopadhyay, R., et al. 2021, The Astrophysical Journal Letters, 922, L11, doi: 10.3847/2041-8213/ac36d1

Huang, J., Kasper, J. C., Fisk, L. A., et al. 2023, The Structure and Origin of Switchbacks: Parker Solar Probe Observations, arXiv, doi: 10.48550/arXiv.2301.10374

Huang, Z., Shi, C., Sioulas, N., & Velli, M. 2022, The Astrophysical Journal, 935, 60, doi: 10.3847/1538-4357/ac74c5

Hunter, J. D. 2007, Computing in Science & Engineering, 9, 90, doi: 10.1109/MCSE.2007.55

Iroshnikov, P. S. 1964, \sovast, 7, 566

Kasper, J. C., Abiad, R., Austin, G., et al. 2016, ßr, 204, 131, doi: 10.1007/s11214-015-0206-3

Kasper, J. C., Klein, K. G., Lichko, E., et al. 2021, Physical Review Letters, 127, 255101, doi: 10.1103/PhysRevLett.127.255101

Keshner, M. 1982, Proceedings of the IEEE, 70, 212, doi: 10.1109/PROC.1982.12282

Kolmogorov, A. 1941, Akademiia Nauk SSSR Doklady, 30, 301

Kraichnan, R. 1965, doi: 10.1063/1.1761412

Laker, R., Horbury, T. S., Bale, S. D., et al. 2021, Astronomy and Astrophysics, 650, A1, doi: 10.1051/0004-6361/202039354

Lam, S. K., Pitrou, A., & Seibert, S. 2015, in Proceedings of the Second Workshop on the LLVM Compiler Infrastructure in HPC (Austin Texas: ACM), 1–6, doi: 10.1145/2833157.2833162

Larosa, A., Krasnoselskikh, V., Wit, T. D. d., et al. 2021, Astronomy & Astrophysics, 650, A3, doi: 10.1051/0004-6361/202039442

Livi, R., Larson, D. E., Kasper, J. C., et al. 2022, The Astrophysical Journal, 938, 138, doi: 10.3847/1538-4357/ac93f5

Magyar, N., & Doorsselaere, T. V. 2022, The Astrophysical Journal, 938, 98, doi: 10.3847/1538-4357/ac8b81

Mallet, A., & Chandran, B. D. G. 2021, Journal of Plasma Physics, 87, 175870601, doi: 10.1017/S0022377821000970

Mallet, A., Squire, J., Chandran, B. D. G., Bowen, T., & Bale, S. D. 2021, The Astrophysical Journal, 918, 62, doi: 10.3847/1538-4357/ac0c12

Martinović, M. M., Klein, K. G., Huang, J., et al. 2021, The Astrophysical Journal, 912, 28, doi: 10.3847/1538-4357/abebe5

Matteini, L., Landi, S., Del Zanna, L., Velli, M., & Hellinger, P. 2010, Geophysical Research Letters, 37, L20101, doi: 10.1029/2010GL044806

Matteini, L., Stansby, D., Horbury, T. S., & Chen, C. H. K. 2018, The Astrophysical Journal, 869, L32, doi: 10.3847/2041-8213/aaf573

Matthaeus, W. H., & Goldstein, M. L. 1986, Physical Review Letters, 57, 495, doi: 10.1103/PhysRevLett.57.495

Meng, M.-M., Liu, Y. D., Chen, C., & Wang, R. 2022, Research in Astronomy and Astrophysics, 22, 035018, doi: 10.1088/1674-4527/ac49e4

Moncuquet, M., Meyer-Vernet, N., Issautier, K., et al. 2020, The Astrophysical Journal Supplement Series, 246, 44, doi: 10.3847/1538-4365/ab5a84

Monin, A. S., & Jaglom, A. M. 1987, Statistical fluid mechanics. 2, 3rd edn. (Cambridge, Mass.: MIT Pr)

Mozer, F. S., Agapitov, O. V., Bale, S. D., et al. 2020, The Astrophysical Journal Supplement Series, 246, 50, doi: 10.3847/1538-4365/ab5e4b

Parker, E. N. 1958, The Astrophysical Journal, 128, 664, doi: 10.1086/146579

Podesta, J. J. 2009, The Astrophysical Journal, 698, 986, doi: 10.1088/0004-637X/698/2/986

Pulupa, M., Bale, S. D., Bonnell, J. W., et al. 2017, Journal of Geophysical Research: Space Physics, 122, 2836, doi: 10.1002/2016JA023345

Raouafi, N. E., Matteini, L., Squire, J., et al. 2023, Space Science Reviews, 219, 8, doi: 10.1007/s11214-023-00952-4

Réville, V., Tenerani, A., & Velli, M. 2018, The Astrophysical Journal, 866, 38, doi: 10.3847/1538-4357/aadb8f

Shi, C. ., Velli, M., Bale, S. D., et al. 2022a, Physics of Plasmas, 29, 122901, doi: 10.1063/5.0124703

Shi, C., Velli, M., Panasenco, O., et al. 2021, Astronomy & Astrophysics, 650, A21, doi: 10.1051/0004-6361/202039818

Shi, C., Panasenco, O., Velli, M., et al. 2022b, The Astrophysical Journal, 934, 152

Shi, M., Li, H., Xiao, C., & Wang, X. 2017, The Astrophysical Journal, 842, 63, doi: 10.3847/1538-4357/aa71b6

Sioulas, N., Huang, Z., Velli, M., et al. 2022, arXiv preprint arXiv:2206.00871

Sioulas, N., Huang, Z., Shi, C., et al. 2023a, The Astrophysical Journal Letters, 943, L8, doi: 10.3847/2041-8213/acaeff

Sioulas, N., Velli, M., Huang, Z., et al. 2023b, On the evolution of the Anisotropic Scaling of Magnetohydrodynamic Turbulence in the Inner Heliosphere, arXiv, doi: 10.48550/arXiv.2301.03896

Sridhar, S., & Goldreich, P. 1994, The Astrophysical Journal, 432, 612, doi: 10.1086/174600

Team, T. P. D. 2023, pandas-dev/pandas: Pandas, Zenodo, doi: 10.5281/ZENODO.3509134

Telloni, D., Sorriso-Valvo, L., Woodham, L. D., et al. 2021, \apjl, 912, L21, doi: 10.3847/2041-8213/abf7d1

Tenerani, A., Sioulas, N., Matteini, L., et al. 2021, The Astrophysical Journal Letters, 919, L31, doi: 10.3847/2041-8213/ac2606

Tenerani, A., & Velli, M. 2013, Journal of Geophysical Research: Space Physics, 118, 7507, doi: 10.1002/2013JA019293

Tenerani, A., Velli, M., & Hellinger, P. 2017, The Astrophysical Journal, 851, 99, doi: 10.3847/1538-4357/aa9bef

Tenerani, A., Velli, M., Matteini, L., et al. 2020, The Astrophysical Journal, 9

Tu, C. Y., & Marsch, E. 1995, Space Science Reviews, 73, 1, doi: 10.1007/BF00748891

Velli, M., Grappin, R., & Mangeney, A. 1989, Physical Review Letters, 63, 1807, doi: 10.1103/PhysRevLett.63.1807

—. 1991, Geophysical & Astrophysical Fluid Dynamics, 62, 101, doi: 10.1080/03091929108229128

Verdini, A., Grappin, R., Pinto, R., & Velli, M. 2012, The Astrophysical Journal, 750, L33, doi: 10.1088/2041-8205/750/2/L33

Verdini, A., & Velli, M. 2007, The Astrophysical Journal, 662, 669, doi: 10.1086/510710

Virtanen, P., Gommers, R., Oliphant, T. E., et al. 2020, Nature Methods, 17, 261, doi: 10.1038/s41592-019-0686-2

Whang, Y. C. 1973, Journal of Geophysical Research, 78, 7221, doi: 10.1029/JA078i031p07221

Woolley, T., Matteini, L., Horbury, T. S., et al. 2020, Monthly Notices of the Royal Astronomical Society, 498, 5524, doi: 10.1093/mnras/staa2770

Zank, G. P., Zhao, L.-L., Adhikari, L., et al. 2022, The Astrophysical Journal Letters, 926, L16, doi: 10.3847/2041-8213/ac51da

Zanna, L. D., Matteini, L., Landi, S., Verdini, A., & Velli, M. 2015, Journal of Plasma Physics, 81, 325810102, doi: 10.1017/S0022377814000579